Collecting Scattering Data for Microwave Imaging by means of the Compressive Sensing Technique

G. Oliveri, N. Anselmi, M. Salucci, L. Poli, and A. Massa

2024/09/13

Contents

1 Numerical Results, Part #3: Retrieval of Aggregated Pixels

OBJECTIVE: This Section is aimed to validate the proposed approach when changing the shape of the scatterer assumed to be composed by adjacent/aggregated pixels. The performance in terms of reconstruction accuracy are still evaluated in a comparative fashion with the results obtained obtained when using a *uniform* measurement setup.

Test Case Description

Direct solver:

- Side of the investigation domain: $L = 3.0\lambda$
- Cubic domain divided in $\sqrt{D} \times \sqrt{D}$ cells
- Number of cells for the direct solver: $D = 1600$ (discretization $= \lambda/10$)

Investigation domain:

- Cubic domain divided in $\sqrt{N} \times \sqrt{N}$ cells
- Number of cells for the inversion: $N = 324$

Measurement domain:

- Total number of measurements: $M \in [2 : 38]$
- Measurement points placed on circles of radius $\rho = 3.0\lambda$

Sources:

- Plane waves
- Number of views: $V = 1$; $\theta^v_{inc} = 0\frac{1}{2}$
- Amplitude: $A = 1.0$
- Frequency: $F = 300$ MHz ($\lambda = 1$)

Background:

- $\varepsilon_r = 1.0$
- $\sigma = 0$ [S/m]

Scatterer:

- Scatterers size/sparsity factor: $S = 1, 2, 3, 4$
- Contrast: $\tau = 0.5$

1.1 Aggregated Pixels, $S = 2$, $SNR = 20$ [dB]

Reconstructed Profiles

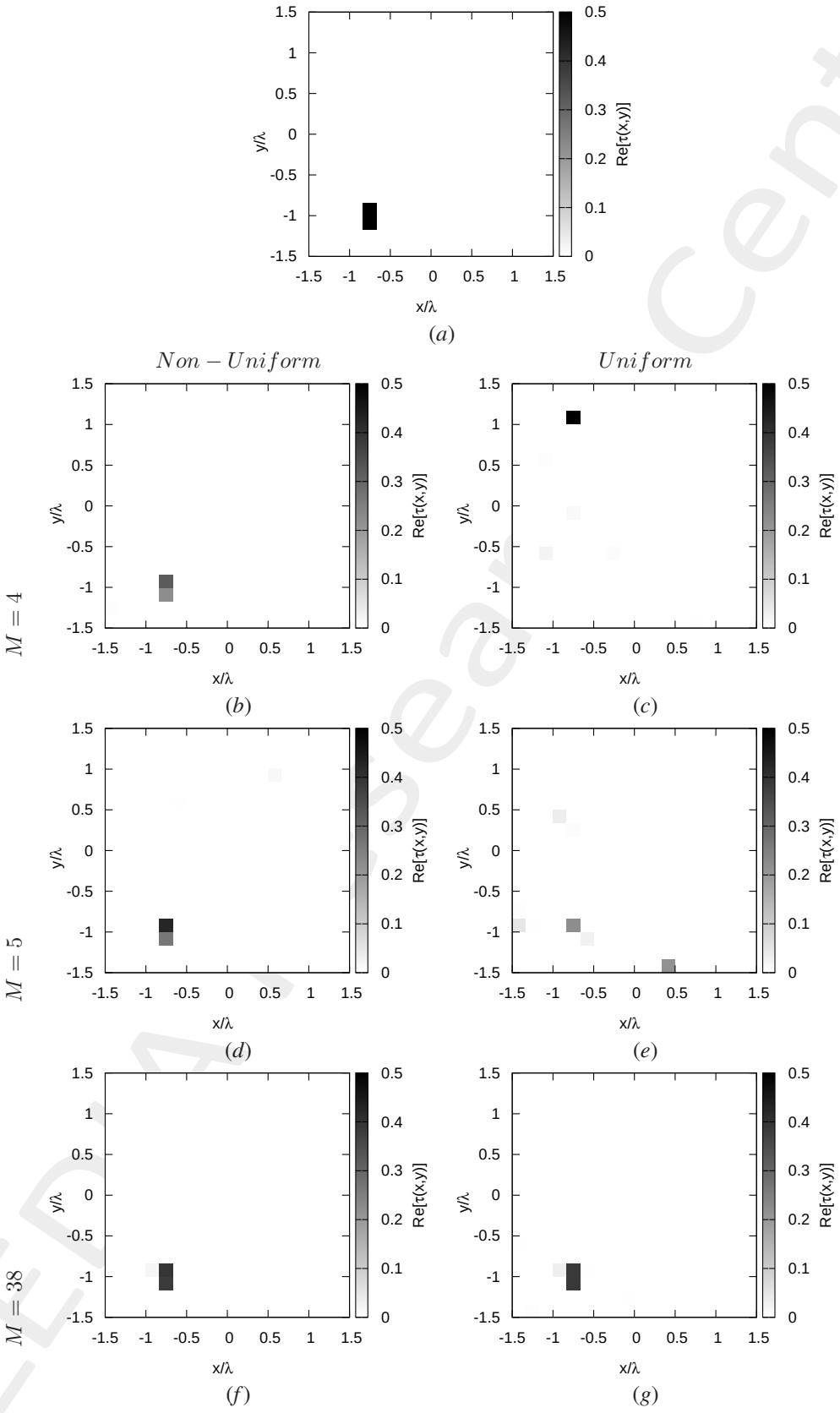

Figure 1: (*a*) Actual and (*b*)(*c*) reconstructed profiles considering (*b*)(*d*)(*f*) non-uniform optimized and (*c*)(*e*)(*g*) uniform measurement setup with (*b*)(*c*) minimum, (*d*)(*e*) intermediate/best and (*f*)(*g*) maximum M.

1.2 Aggregated Pixels, $S = 2$, $SNR = 10$ [dB]

Reconstructed Profiles

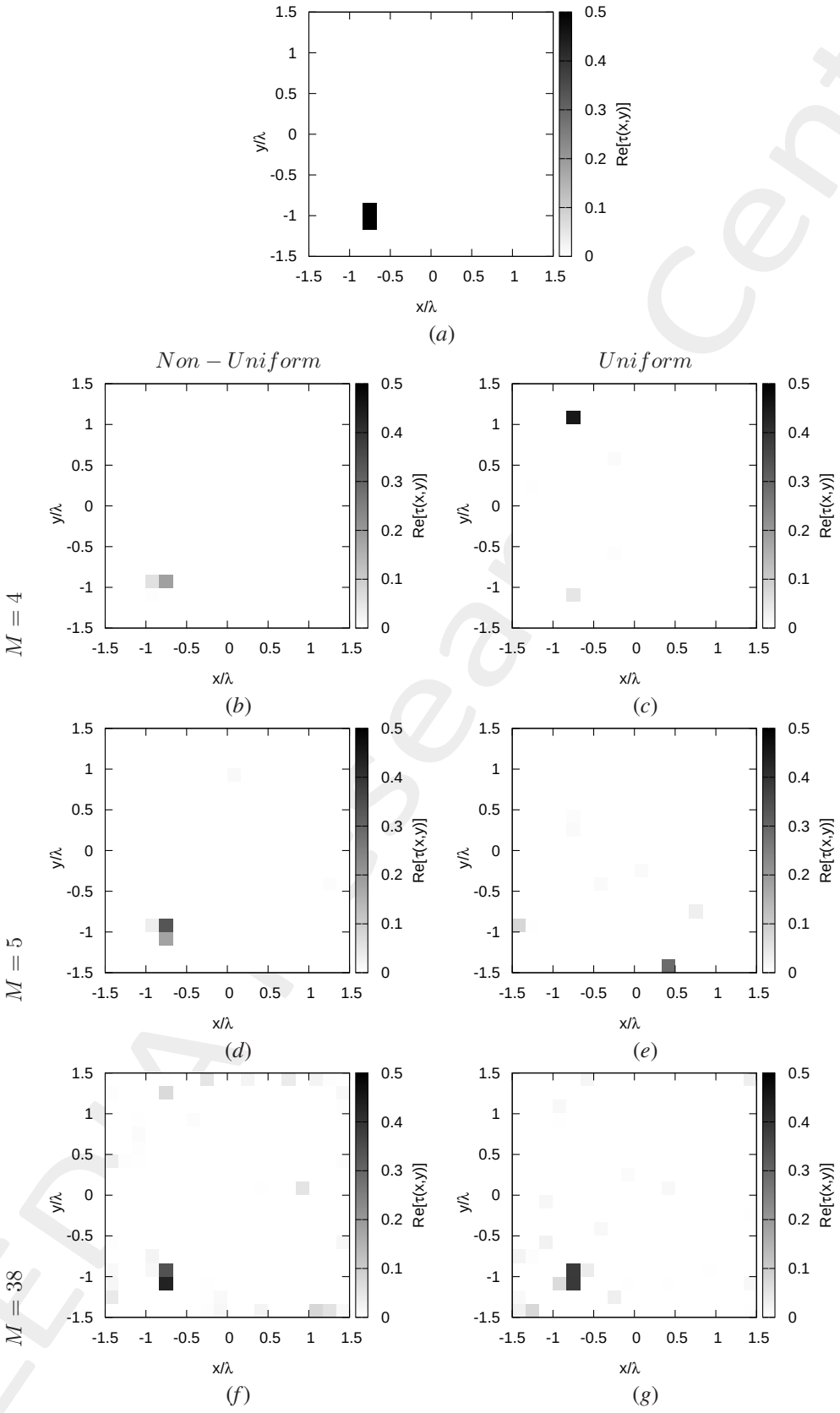

Figure 2: (*a*) Actual and (*b*)(*c*) reconstructed profiles considering (*b*)(*d*)(*f*) non-uniform optimized and (*c*)(*e*)(*g*) uniform measurement setup with (*b*)(*c*) minimum, (*d*)(*e*) intermediate/best and (*f*)(*g*) maximum M.

1.3 Aggregated Pixels, $S = 3$, $SNR = 10$ [dB]

Reconstructed Profiles

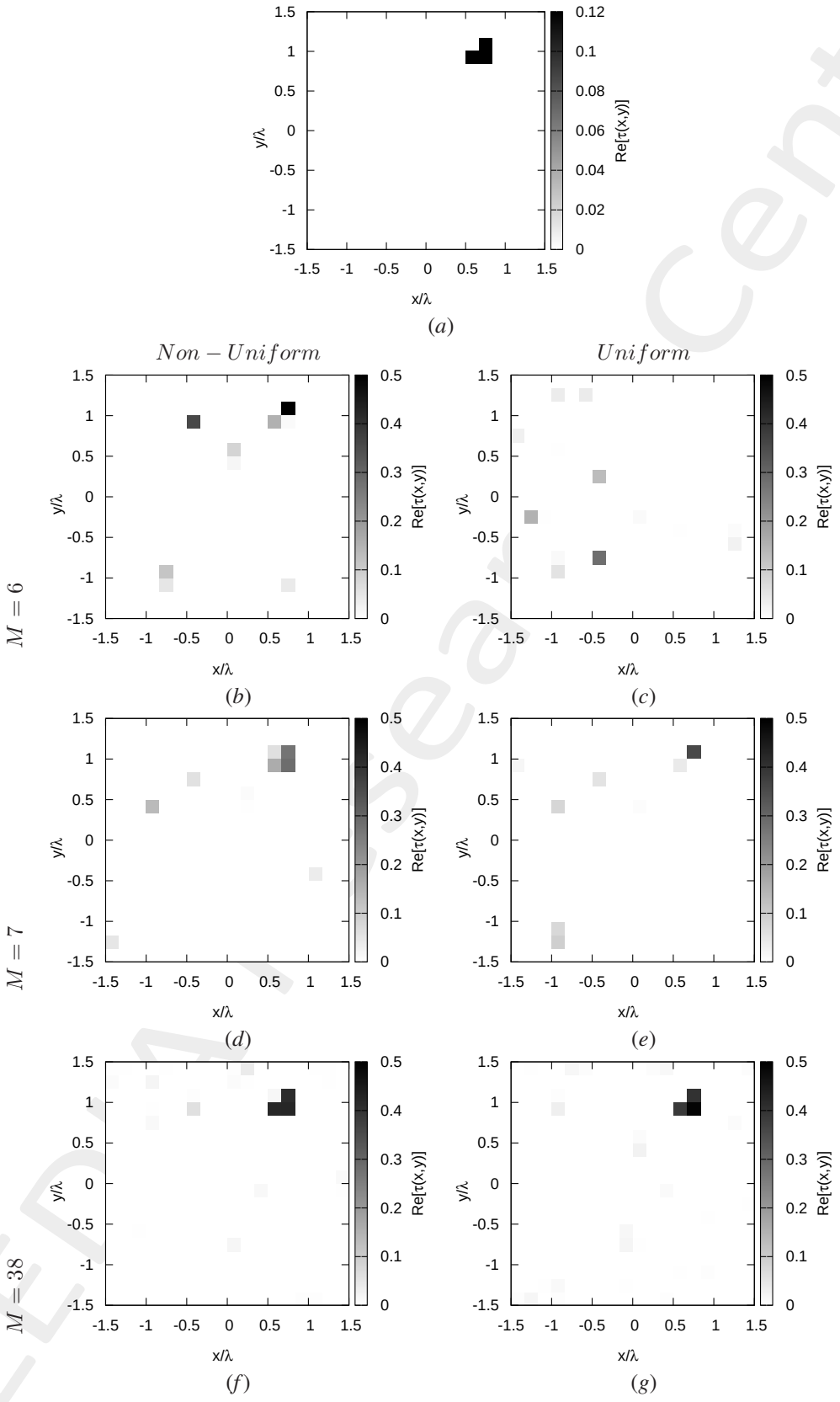

Figure 3: (*a*) Actual and (*b*)(*c*) reconstructed profiles considering (*b*)(*d*)(*f*) non-uniform optimized and (*c*)(*e*)(*g*) uniform measurement setup with (*b*)(*c*) minimum, (*d*)(*e*) intermediate/best and (*f*)(*g*) maximum M.

Resume Error Figures - Total, Internal and External Errors vs. M

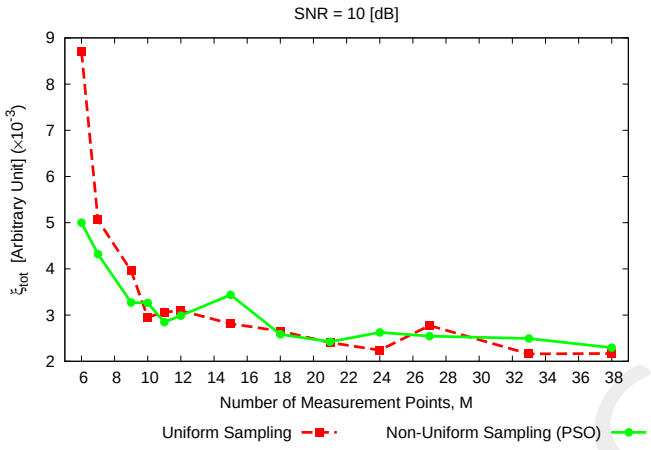

(*a*)

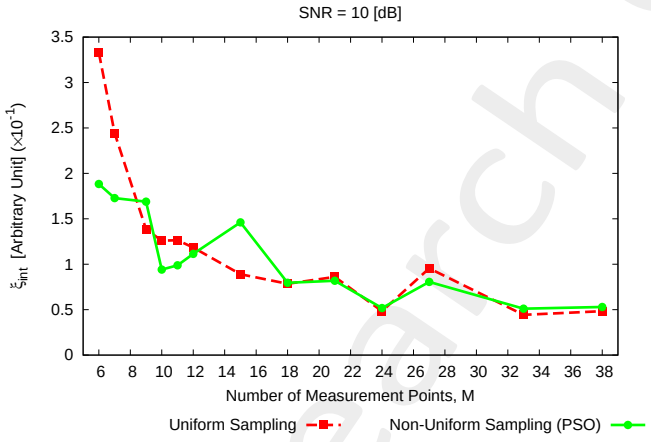

(*b*)

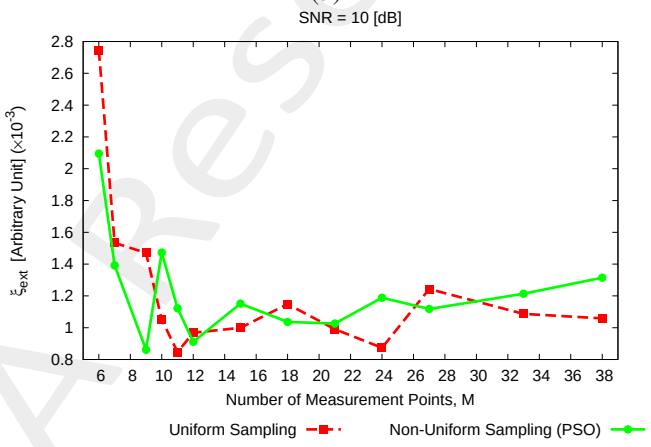

(*c*)

Figure 4: (*a*) Total, (*b*) internal and (*c*) external reconstruction errors vs. number of measurement points M shown in a comparative fashion with those obtained when using a *uniform* measurement setup.

1.4 Aggregated Pixels, $S = 4$, $SNR = 20$ [dB]

Reconstructed Profiles

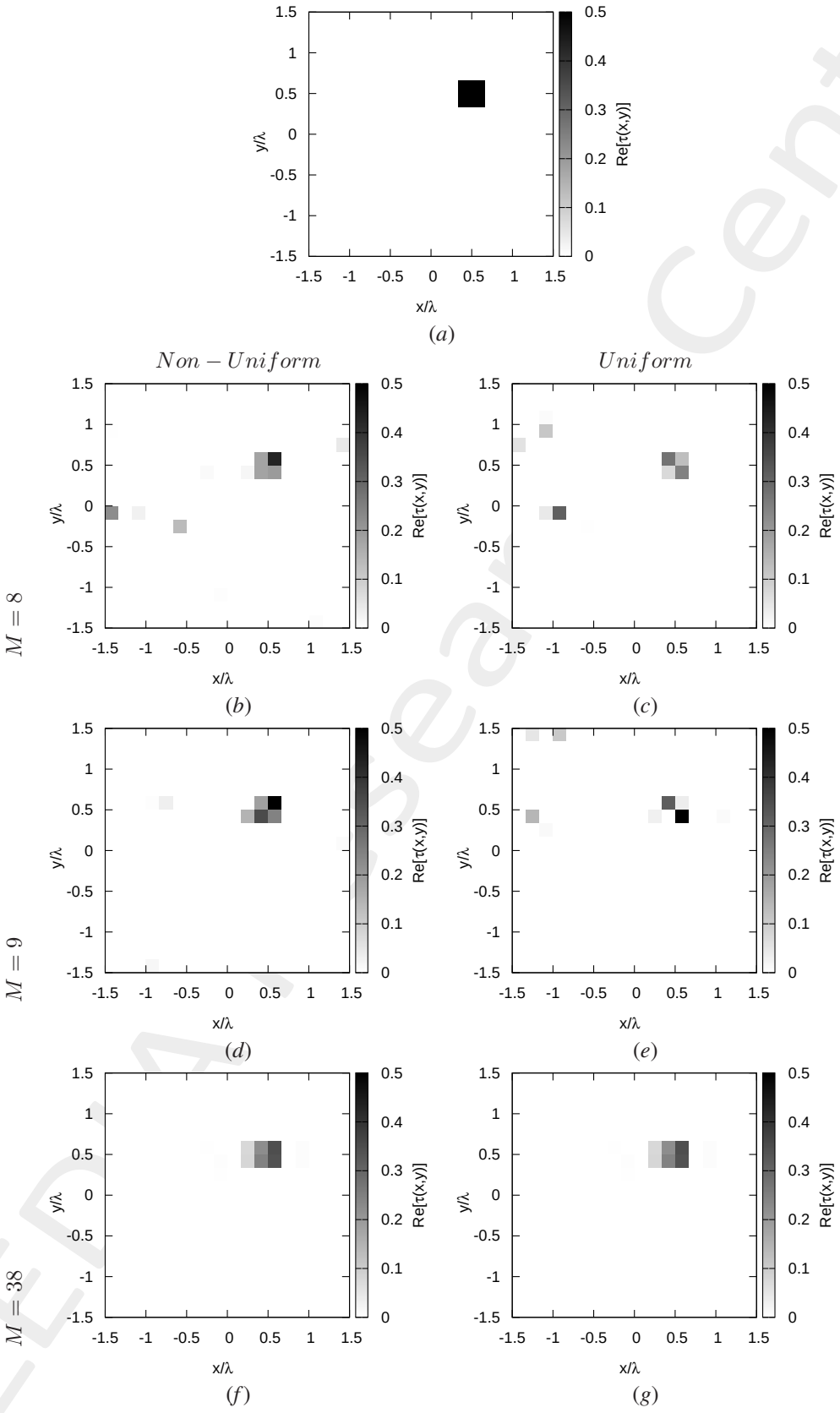

Figure 5: (a) Actual and (b)(c) reconstructed profiles considering (b)(d)(f) non-uniform optimized and (c)(e)(g) uniform measurement setup with (b)(c) minimum, (d)(e) intermediate/best and (f)(g) maximum M.

Resume Error Figures - Total, Internal and External Errors vs. M

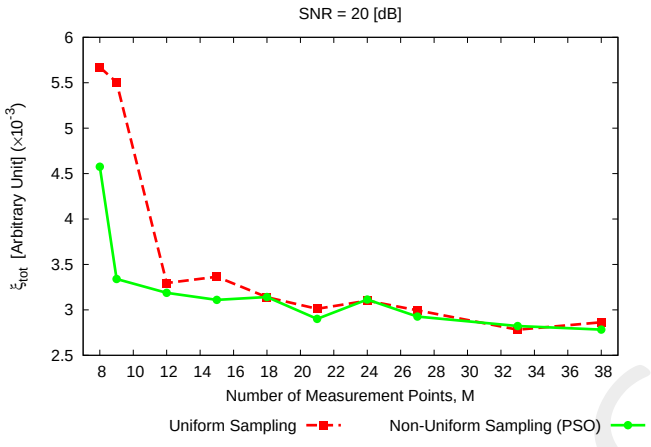

(*a*)

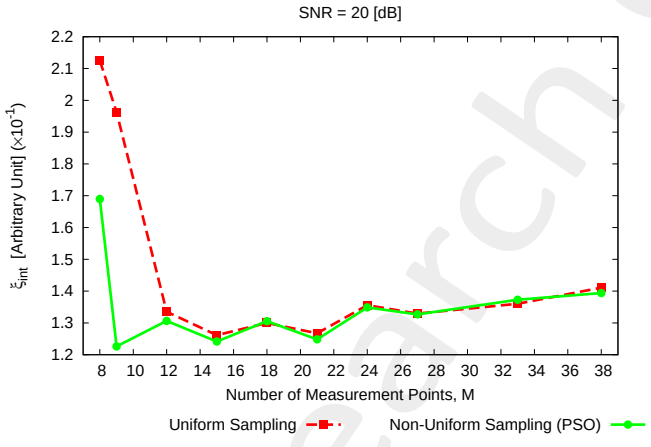

(*b*)

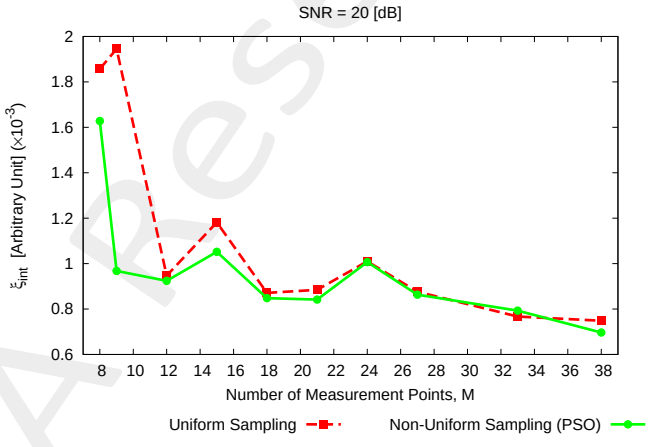

(*c*)

Figure 6: (*a*) Total, (*b*) internal and (*c*) external reconstruction errors vs. number of measurement points M shown in a comparative fashion with those obtained when using a *uniform* measurement setup.

1.5 Aggregated Pixels, $S = 4$, $SNR = 10$ [dB]

Reconstructed Profiles

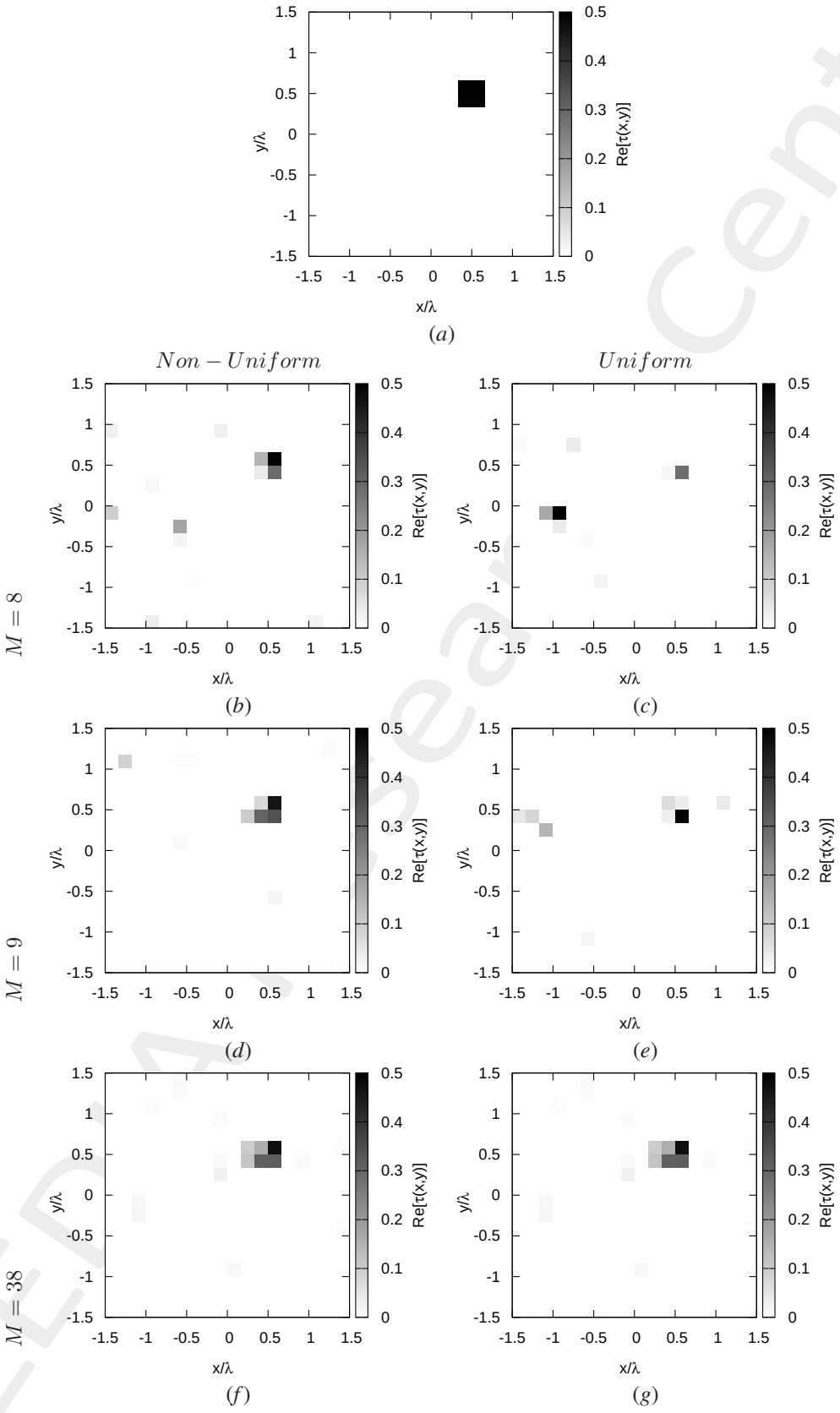

Figure 7: (a) Actual and (b)(c) reconstructed profiles considering (b)(d)(f) non-uniform optimized and (c)(e)(g) uniform measurement setup with (b)(c) minimum, (d)(e) intermediate/best and (f)(g) maximum M.

Resume Error Figures - Total, Internal and External Errors vs. M

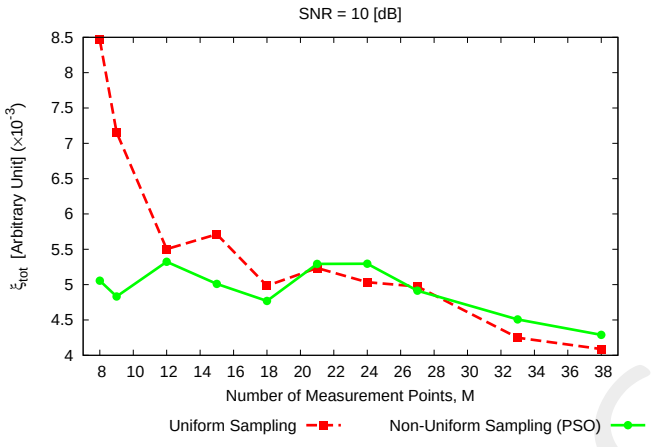

(*a*)

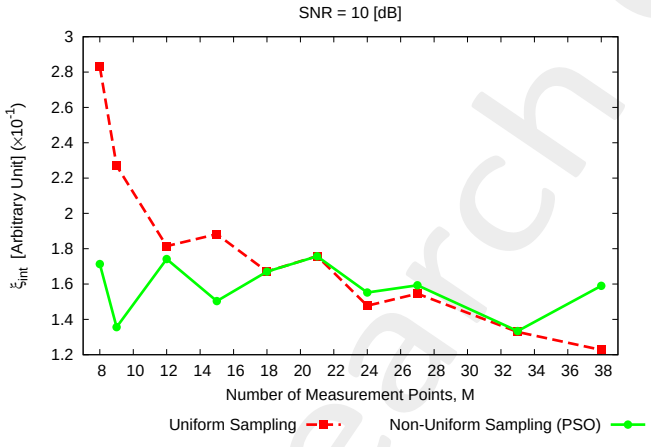

(*b*)

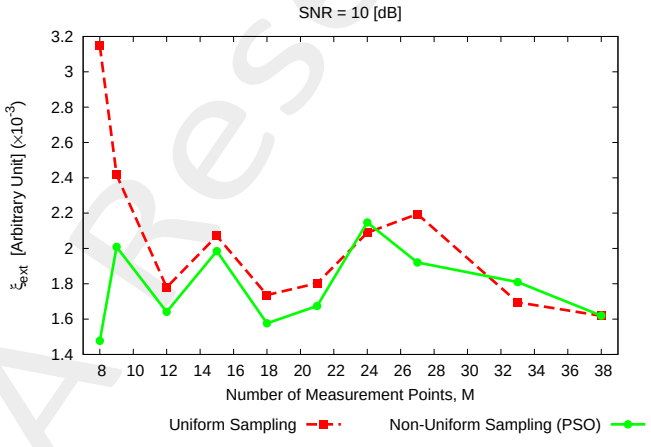

(*c*)

Figure 8: (*a*) Total, (*b*) internal and (*c*) external reconstruction errors vs. number of measurement points M shown in a comparative fashion with those obtained when using a *uniform* measurement setup.

1.6 Analysis vs. S

1.6.1 Non-Aggregated Pixels

OBJECTIVE: This Section is aimed to validate the proposed approach when increasing S. The performance in terms of reconstruction accuracy are still evaluated in a comparative fashion with the results obtained obtained when using a *uniform* measurement setup.

Test Case Description

Direct solver:

- Side of the investigation domain: $L = 3.0\lambda$
- Cubic domain divided in $\sqrt{D} \times \sqrt{D}$ cells
- Number of cells for the direct solver: $D = 1600$ (discretization $= \lambda/10$)

Investigation domain:

- Cubic domain divided in $\sqrt{N} \times \sqrt{N}$ cells
- Number of cells for the inversion: $N = 324$

Measurement domain:

- Total number of measurements: $M \in [2 : 38]$
- Measurement points placed on circles of radius $\rho = 3.0\lambda$

Sources:

- Plane waves
- Number of views: $V = 1$; $\theta_{inc}^{v} = 0\frac{1}{2}$
- Amplitude: $A = 1.0$
- Frequency: $F = 300$ MHz ($\lambda = 1$)

Background:

- $\varepsilon_r = 1.0$
- $\sigma = 0$ [S/m]

Scatterer:

- Scatterers size/sparsity factor: $S = 1, 2, 3, 4, 5$
- Contrast: $\tau = 0.5$

$S \in [1:5]$, $M = 2 \times S + 1$

Resume Error Figures - Total, Internal and External Errors vs. S for $SNR = 20$ [dB]

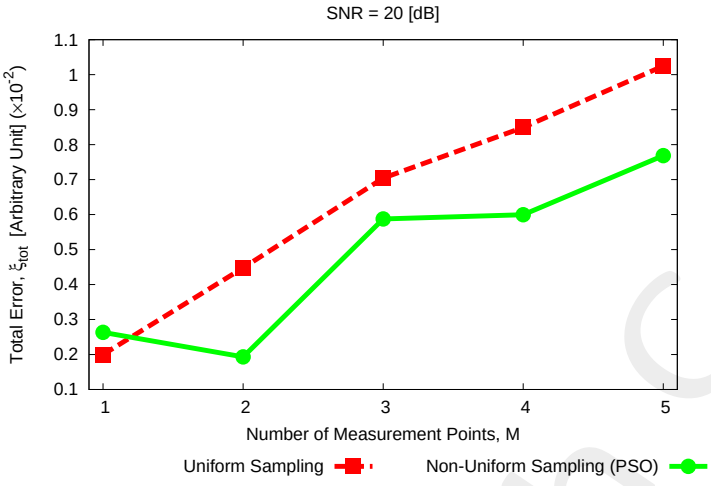

(*a*)

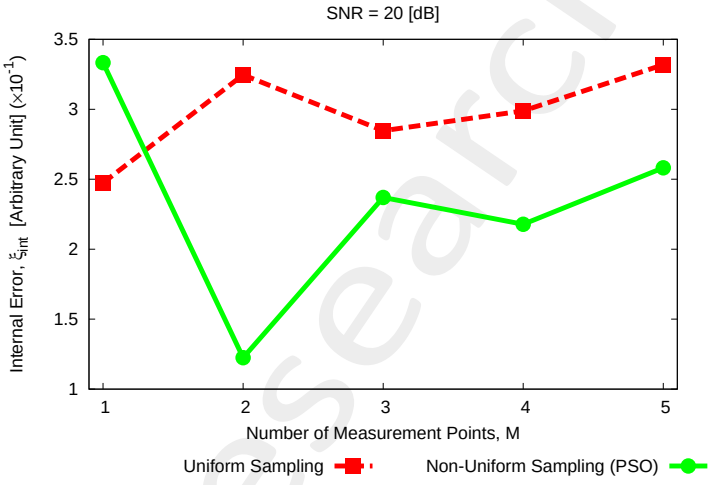

(*b*)

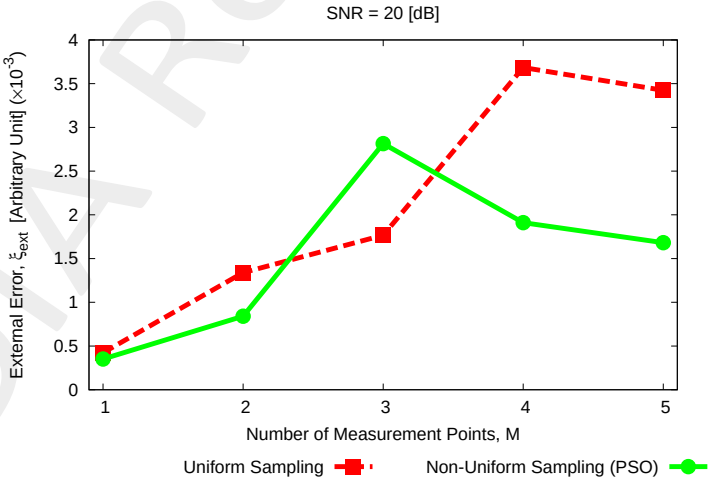

(*d*)

Figure 9: (*a*) Total, (*b*) internal and (*c*) external reconstruction error vs. contrast τ of the single-pixel scatterer.

Resume Error Figures - Total, Internal and External Errors vs. S for $SNR = 10$ [dB]

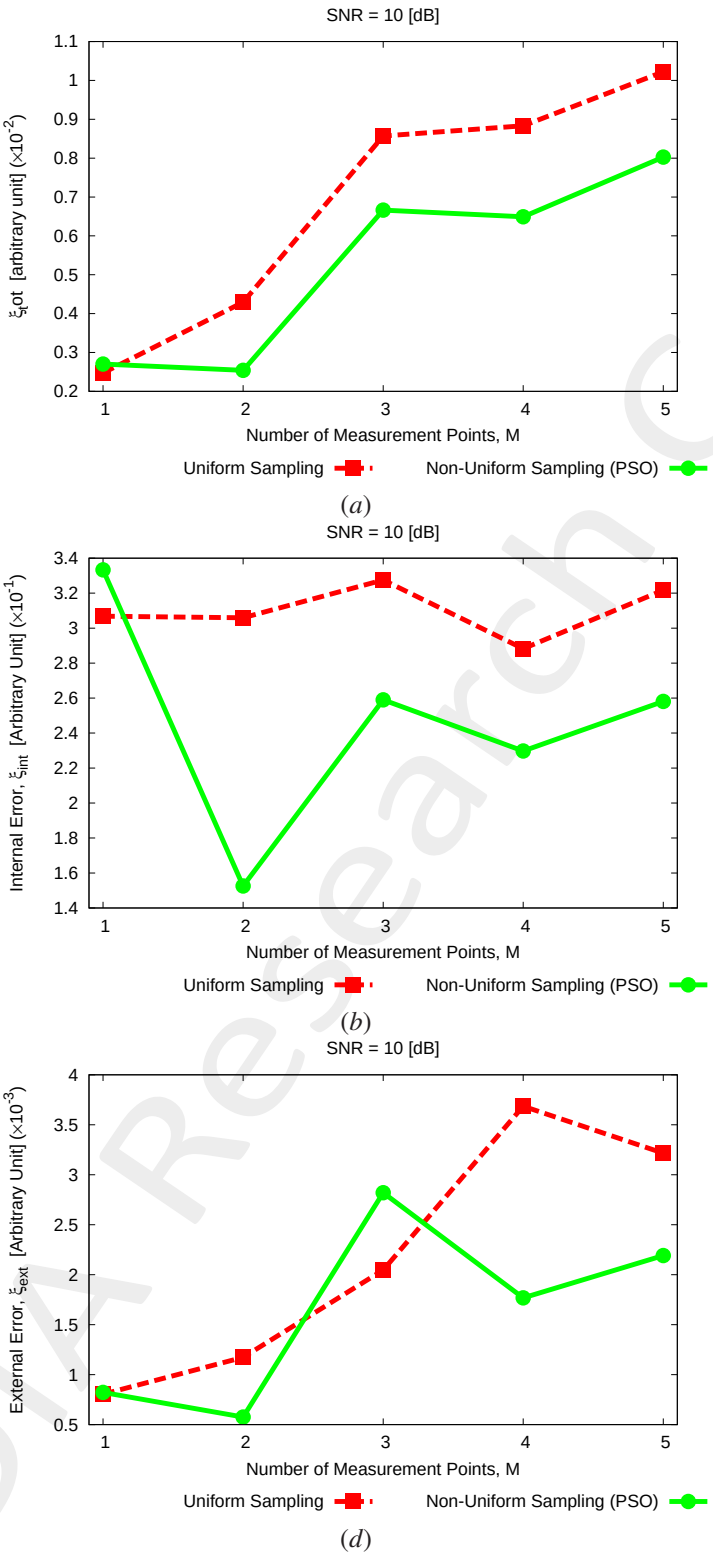

Figure 10: (*a*) Total, (*b*) internal and (*c*) external reconstruction error vs. contrast τ of the single-pixel scatterer.

1.6.2 Aggregated Pixels

OBJECTIVE: This Section is aimed to validate the proposed approach when increasing S. The performance in terms of reconstruction accuracy are still evaluated in a comparative fashion with the results obtained obtained when using a *uniform* measurement setup.

Test Case Description

Direct solver:

- Side of the investigation domain: $L = 3.0\lambda$
- Cubic domain divided in $\sqrt{D} \times \sqrt{D}$ cells
- Number of cells for the direct solver: $D = 1600$ (discretization $= \lambda/10$)

Investigation domain:

- Cubic domain divided in $\sqrt{N} \times \sqrt{N}$ cells
- Number of cells for the inversion: $N = 324$

Measurement domain:

- Total number of measurements: $M \in [2 : 38]$
- Measurement points placed on circles of radius $\rho = 3.0\lambda$

Sources:

- Plane waves
- Number of views: $V = 1$; $\theta^v_{inc} = 0\frac{1}{2}$
- Amplitude: $A = 1.0$
- Frequency: $F = 300$ MHz ($\lambda = 1$)

Background:

- $\varepsilon_r = 1.0$
- $\sigma = 0$ [S/m]

Scatterer:

- Scatterers size/sparsity factor: $S = 1, 2, 3, 4, 5$
- Contrast: $\tau = 0.5$

$S \in [1:4]$, $M = 2 \times S$

Resume Error Figures - Total, Internal and External Errors vs. S for $SNR = 20$ [dB]

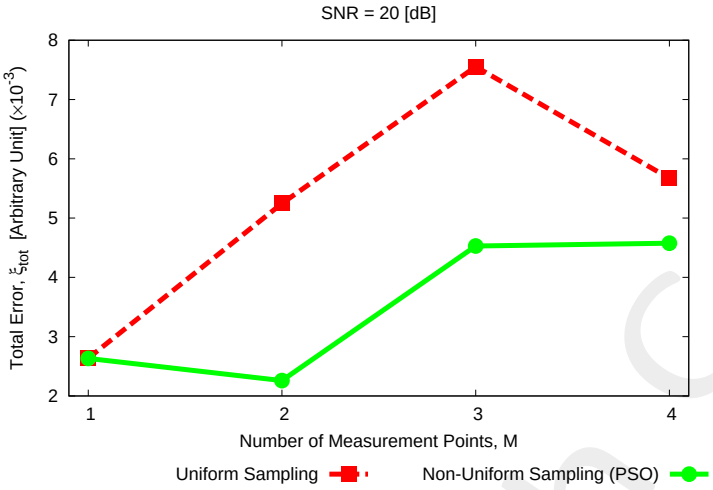

(*a*)

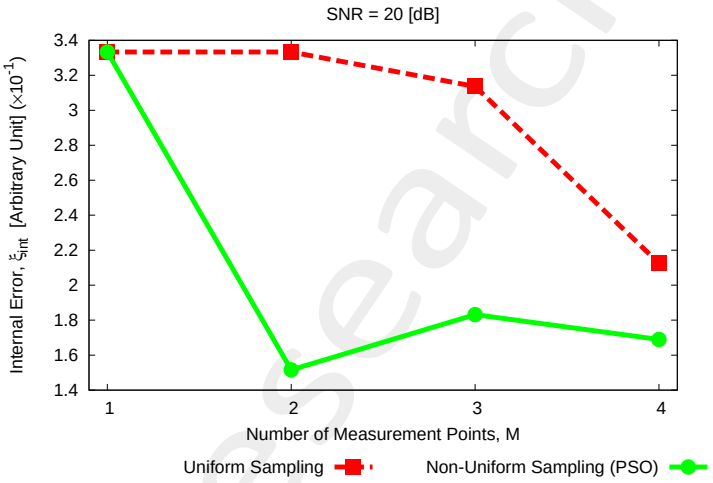

(*b*)

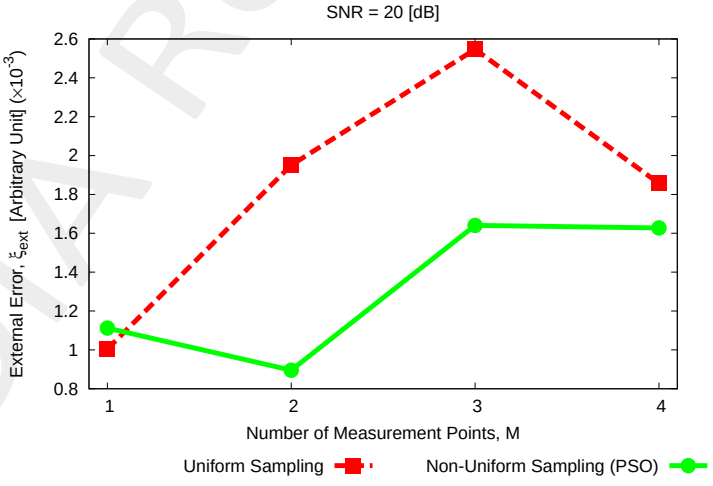

(*d*)

Figure 11: (*a*) Total, (*b*) internal and (*c*) external reconstruction error vs. contrast τ of the single-pixel scatterer.

Resume Error Figures - Total, Internal and External Errors vs. S for $SNR = 10$ [dB]

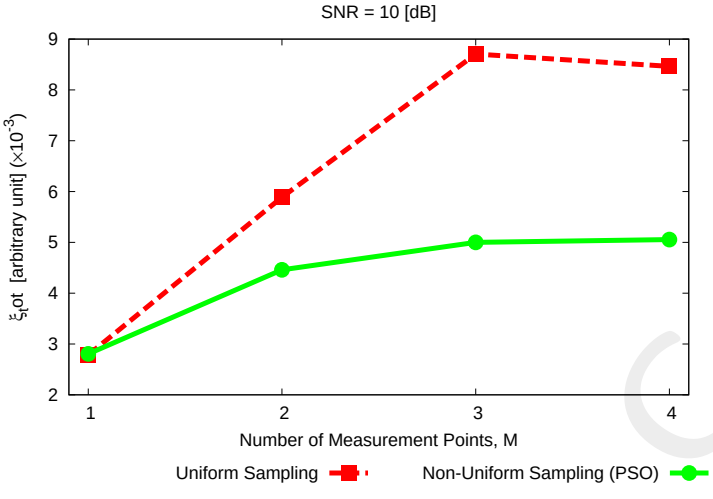

(*a*)

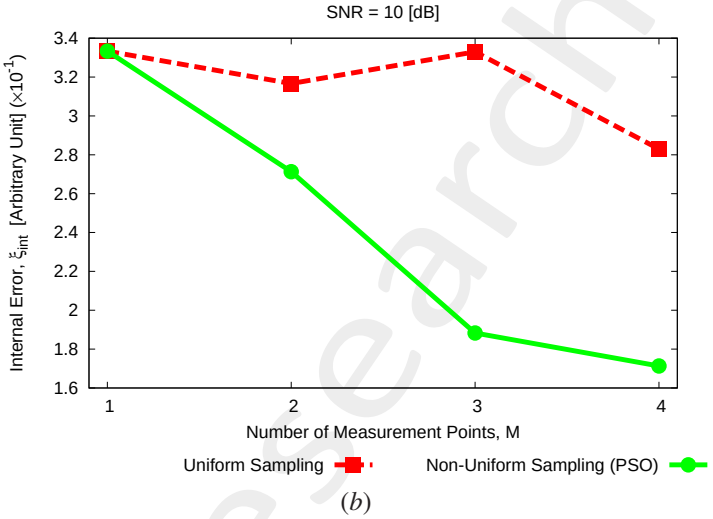

(*b*)

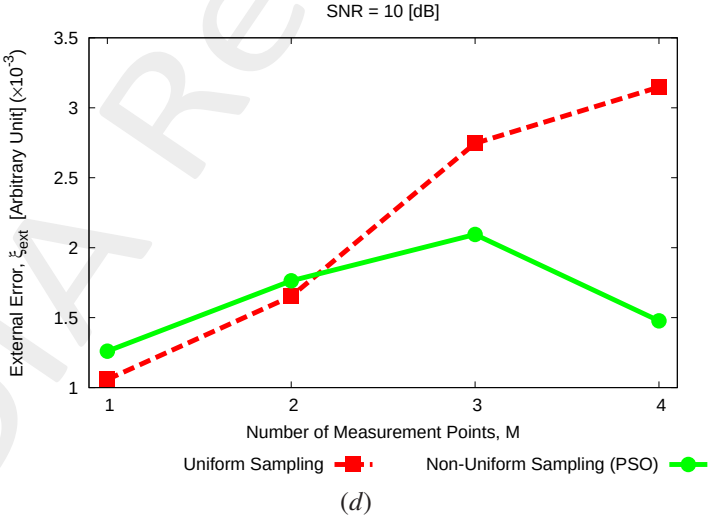

(*d*)

Figure 12: (*a*) Total, (*b*) internal and (*c*) external reconstruction error vs. contrast τ of the single-pixel scatterer.

$S \in [1:4]$, $M = 2 \times S + 1$

Resume Error Figures - Total, Internal and External Errors vs. S for $SNR = 20$ [dB]

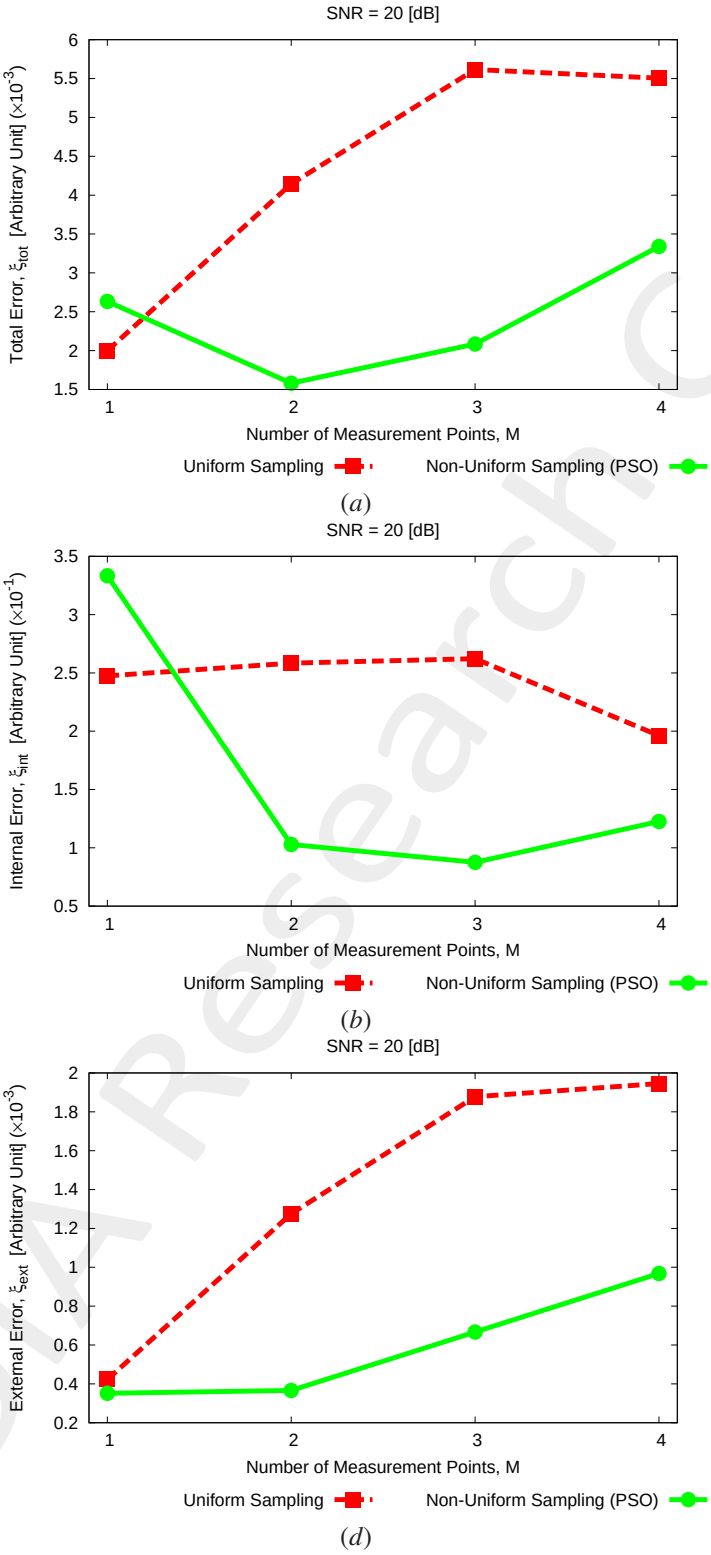

Figure 13: (*a*) Total, (*b*) internal and (*c*) external reconstruction error vs. contrast τ of the single-pixel scatterer.

Resume Error Figures - Total, Internal and External Errors vs. S for $SNR = 10$ [dB]

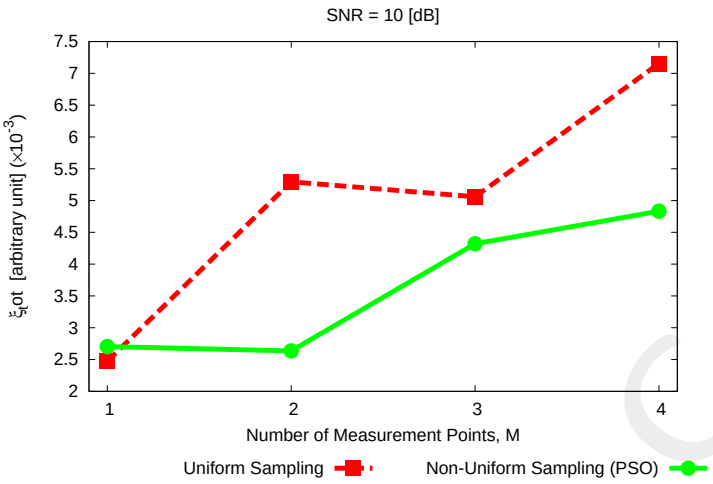

(*a*)

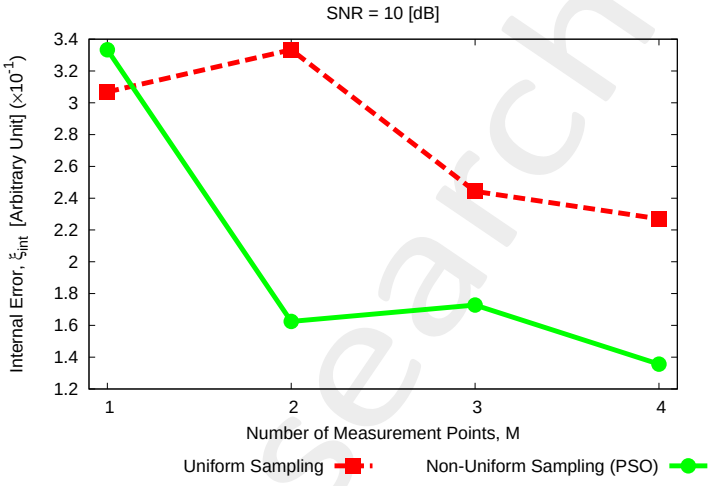

(*b*)

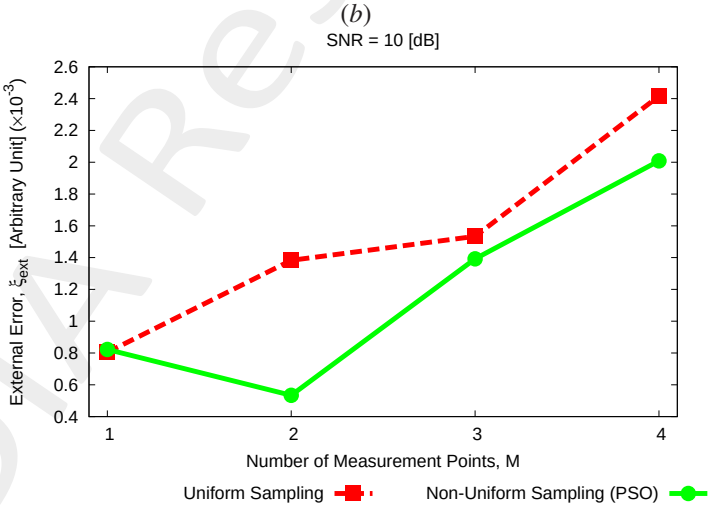

(*d*)

Figure 14: (*a*) Total, (*b*) internal and (*c*) external reconstruction error vs. contrast τ of the single-pixel scatterer.

OUTCOMES:

- If the scattered field samples are collected by the sensor placed within the observation domain according to the non-

uniform optimized distributions the reconstruction errors are generally lower (or almost equal in some cases) than those obtained considering a conventional uniform distribution (in which the sensor are equally-spaced), whatever the number of pixels S.

1.7 Analysis vs. Contrast, τ

OBJECTIVE: This Section is aimed to validate the proposed approach when increasing the contrast τ. The performance in terms of reconstruction accuracy are still evaluated in a comparative fashion with the results obtained obtained when using a *uniform* measurement setup.

Test Case Description

Direct solver:

- Side of the investigation domain: $L = 3.0\lambda$
- Cubic domain divided in $\sqrt{D} \times \sqrt{D}$ cells
- Number of cells for the direct solver: $D = 1600$ (discretization $= \lambda/10$)

Investigation domain:

- Cubic domain divided in $\sqrt{N} \times \sqrt{N}$ cells
- Number of cells for the inversion: $N = 324$

Measurement domain:

- Total number of measurements: $M \in [2 : 38]$
- Measurement points placed on circles of radius $\rho = 3.0\lambda$

Sources:

- Plane waves
- Number of views: $V = 1$; $\theta_{inc}^{v} = 0\frac{1}{2}$
- Amplitude: $A = 1.0$
- Frequency: $F = 300$ MHz ($\lambda = 1$)

Background:

- $\varepsilon_r = 1.0$
- $\sigma = 0$ [S/m]

Scatterer:

- Scatterers size/sparsity factor: $S = 3$
- Contrast: $\tau = [0.1 : 2.0]$

1.7.1 Aggregated Pixels, $S = 3$, $\tau = 1.0$, $SNR = 20$ [dB]

Reconstructed Profiles

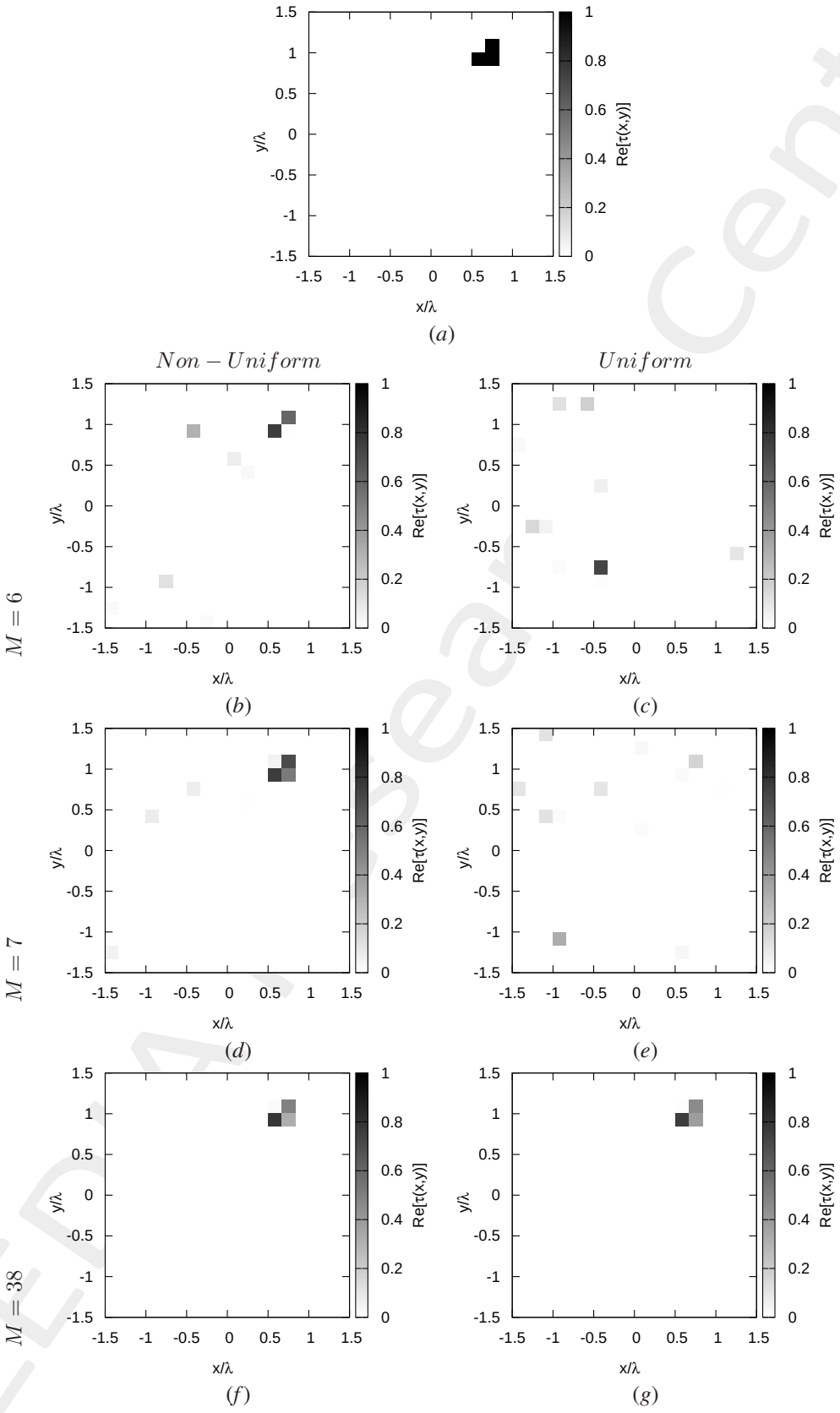

Figure 15: (*a*) Actual and (*b*)(*c*) reconstructed profiles considering (*b*)(*d*)(*f*) non-uniform optimized and (*c*)(*e*)(*g*) uniform measurement setup with (*b*)(*c*) minimum, (*d*)(*e*) intermediate/best and (*f*)(*g*) maximum M.

1.7.2 Aggregated Pixels, $S = 3$, $\tau = 1.0$, $SNR = 10$ [dB]

Reconstructed Profiles

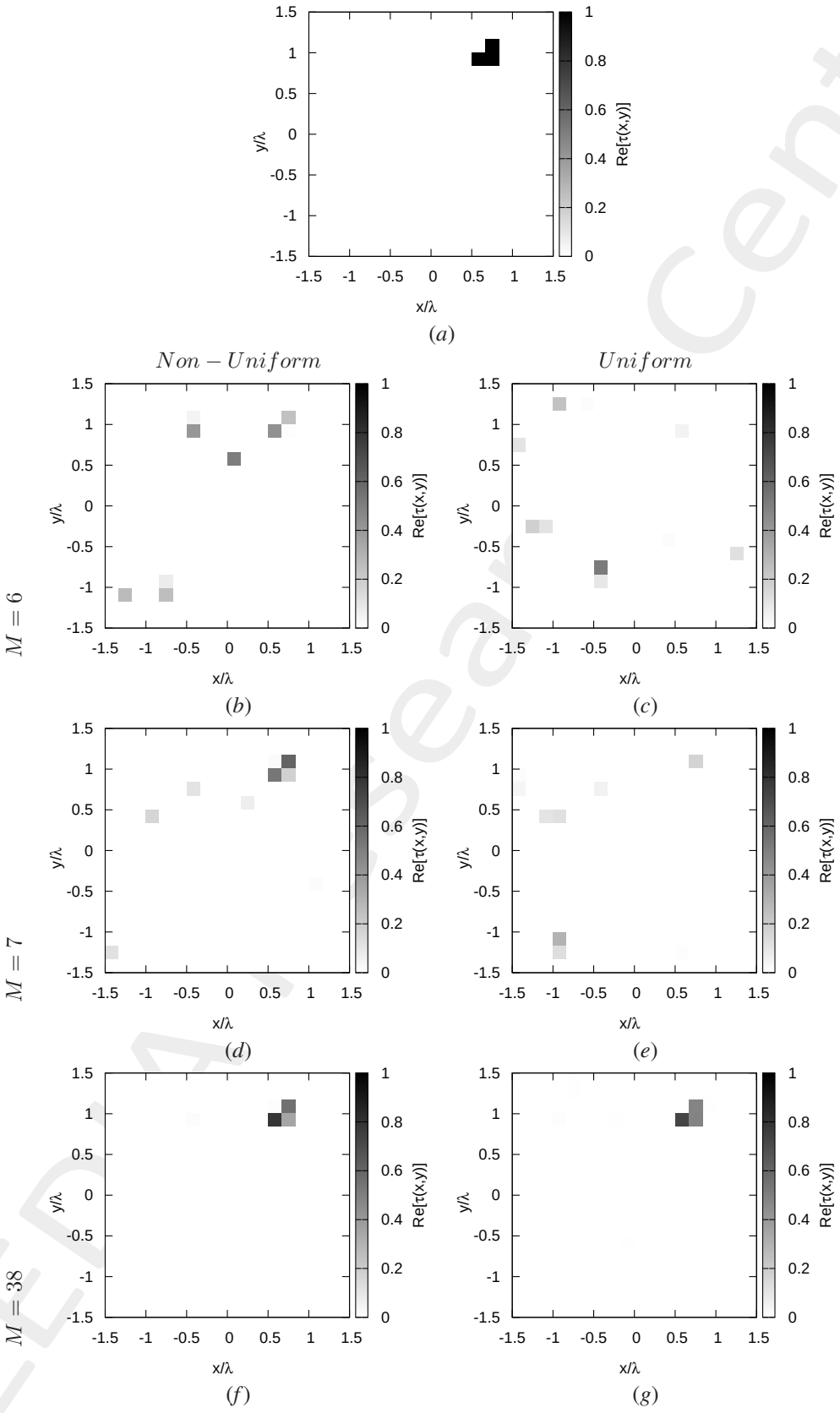

Figure 16: (*a*) Actual and (*b*)(*c*) reconstructed profiles considering (*b*)(*d*)(*f*) non-uniform optimized and (*c*)(*e*)(*g*) uniform measurement setup with (*b*)(*c*) minimum, (*d*)(*e*) intermediate/best and (*f*)(*g*) maximum M.

1.7.3 Aggregated Pixels, $S = 3$, $\tau = 1.5$, $SNR = 20$ [dB]

Reconstructed Profiles

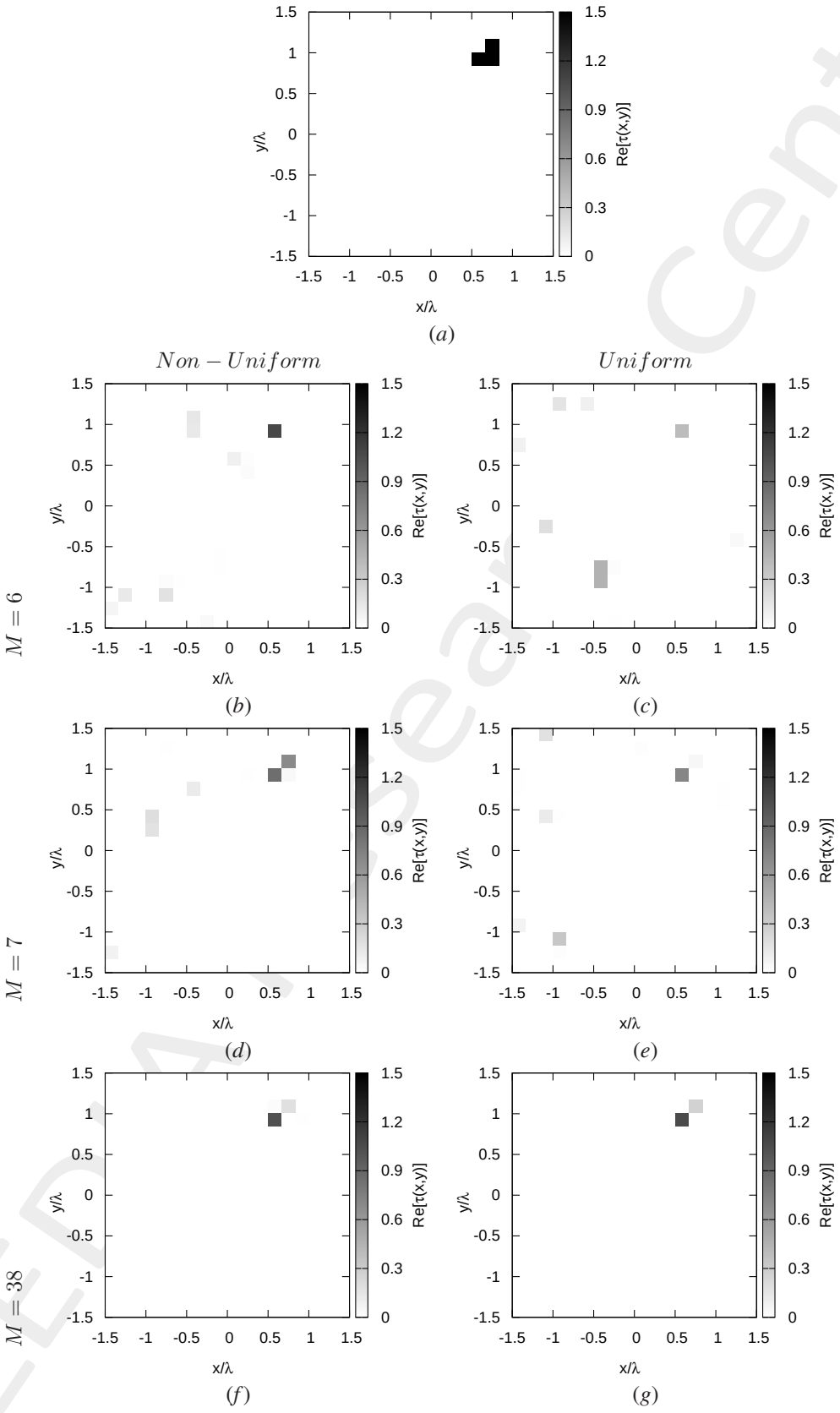

Figure 17: (*a*) Actual and (*b*)(*c*) reconstructed profiles considering (*b*)(*d*)(*f*) non-uniform optimized and (*c*)(*e*)(*g*) uniform measurement setup with (*b*)(*c*) minimum, (*d*)(*e*) intermediate/best and (*f*)(*g*) maximum M.

1.7.4 Aggregated Pixels, $S = 3$, $\tau = 1.5$, $SNR = 10$ [dB]

Reconstructed Profiles

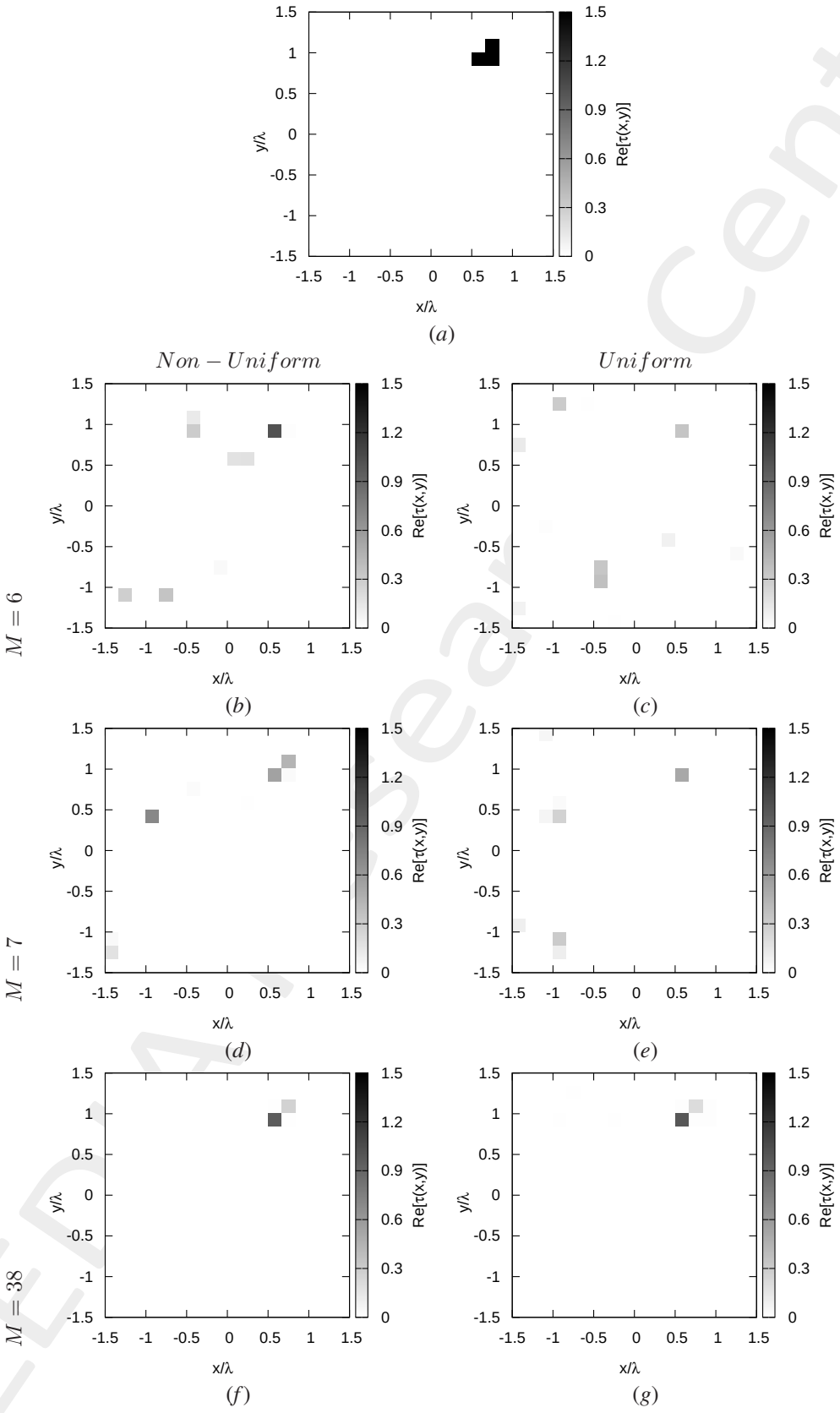

Figure 18: (a) Actual and (b)(c) reconstructed profiles considering (b)(d)(f) non-uniform optimized and (c)(e)(g) uniform measurement setup with (b)(c) minimum, (d)(e) intermediate/best and (f)(g) maximum M.

More information on the topics of this document can be found in the following list of references.

References

[1] M. Salucci, L. Poli, and G. Oliveri, "Full-vectorial 3D microwave imaging of sparse scatterers through a multi-task Bayesian compressive sensing approach," *Journal of Imaging*, vol. 5, no. 1, pp. 1-24, Jan. 2019.

[2] M. Salucci, A. Gelmini, L. Poli, G. Oliveri, and A. Massa, "Progressive compressive sensing for exploiting frequency-diversity in GPR imaging," *J. Electromagn. Waves Appl. J*, vol. 32, no. 9, pp. 1164-1193, 2018.

[3] G. Oliveri, P.-P. Ding, and L. Poli "3D crack detection in anisotropic layered media through a sparseness-regularized solver,"IEEE Antennas Wireless Propag. Lett., vol. 14, pp. 1031-1034, 2015.

[4] Y. Zhong, F. Zardi, M. Salucci, G. Oliveri, and A. Massa, "Multiscaling differential contraction integral method for inverse scattering problems with inhomogeneous media," *IEEE Trans. Microw. Theory Tech.*, vol. 71, no. 9, pp. 4064-4079, Sep. 2023.

[5] X. Ye, F. Zardi, M. Salucci, and A. Massa, "Multiresolution subspace-based optimization method for the retrieval of 2-D perfect electric conductors," *IEEE Trans. Microw. Theory Tech.*, vol. 71, no. 4, pp. 1732-1744, Apr. 2023.

[6] G. Oliveri, N. Anselmi, M. Salucci, L. Poli, and A. Massa, "Compressive sampling-based scattering data acquisition in microwave imaging," *J. Electromagn. Waves Appl. J*, vol. 37, no. 5, 693-729, Mar. 2023.

[7] M. Salucci, L. Poli, P. Rocca, and A. Massa, "Learned global optimization for inverse scattering problems - Matching global search with computational efficiency," *IEEE Trans. Antennas Propag.*, vol. 70, no. 8, pp. 6240-6255, Aug. 2022.

[8] Y. Zhong, M. Salucci, K. Xu, A. Polo, and A. Massa, "A multi-resolution contraction integral equation method for solving highly non-linear inverse scattering problems," *IEEE Trans. Microw. Theory Tech.*, vol. 68, no. 4, pp. 1234-1247, Apr. 2020.

[9] G. Oliveri, L. Poli, N. Anselmi, M. Salucci, and A. Massa, "Compressive sensing-based Born iterative method for tomographic imaging," *IEEE Tran. Microw. Theory Techn.*, vol. 67, no. 5, pp. 1753-1765, May 2019.

[10] N. Anselmi, L. Poli, G. Oliveri, and A. Massa, "Iterative multi-resolution bayesian CS for microwave imaging," *IEEE Trans. Antennas Propag.*, vol. 66, no. 7, pp. 3665-3677, Jul. 2018.

[11] G. Oliveri, M. Salucci, and N. Anselmi, "Tomographic imaging of sparse low-contrast targets in harsh environments through matrix completion," *IEEE Trans. Microw. Theory Tech.*, vol. 66, no. 6, pp. 2714-2730, Jun. 2018.

[12] G. Oliveri, M. Salucci, N. Anselmi, and A. Massa, "Compressive sensing as applied to inverse problems for imaging: theory, applications, current trends, and open challenges," *IEEE Antennas Propag. Mag.*, vol. 59, no. 5, pp. 34-46, Oct. 2017.

[13] N. Anselmi, G. Oliveri, M. A. Hannan, M. Salucci, and A. Massa, "Color compressive sensing imaging of arbitrary-shaped scatterers," *IEEE Trans. Microw. Theory Techn.*, vol. 65, no. 6, pp. 1986-1999, Jun. 2017.

[14] T. Moriyama, M. Salucci, M. Tanaka, and T. Takenaka, "Image reconstruction from total electric field data with no information on the incident field," *J. Electromagn. Waves Appl. J*, vol. 30, no. 9, pp. 1162-1170, 2016.

[15] N. Anselmi, G. Oliveri, M. Salucci, and A. Massa, "Wavelet-based compressive imaging of sparse targets," *IEEE Trans. Antennas Propag.*, vol. 63, no. 11, pp. 4889-4900, Nov. 2015.

[16] X. Ye, L. Poli, G. Oliveri, Y. Zhong, K. Agarwal, A. Massa, and X. Chen,"Multi-resolution subspace-based optimization method for solving three-dimensional inverse scattering problems," *J. Opt. Soc. America A*, vol. 32, no. 11, pp. 2218-2226, Nov. 2015.

[17] G. Oliveri, N. Anselmi, and A. Massa, "Compressive sensing imaging of non-sparse 2D scatterers by a total-variation approach within the Born approximation," *IEEE Trans. Antennas Propag.*, vol. 62, no. 10, pp. 5157-5170, Oct. 2014.

[18] T. Moriyama, G. Oliveri, M. Salucci, and T. Takenaka, "A multi-scaling forward-backward time-stepping method for microwave imaging," *IEICE Electronics Express*, vol. 11, no. 16, pp. 1-12, Aug. 2014.

[19] L. Poli, G. Oliveri, P.-P. Ding, T. Moriyama, and A. Massa, "Multifrequency Bayesian compressive sensing methods for microwave imaging," *J. Opt. Soc. America A*, vol. 31, no. 11, pp. 2415-2428, 2014.

[20] L. Poli, G. Oliveri, and A. Massa, "Imaging sparse metallic cylinders through a Local Shape Function Bayesian Compressive Sensing approach," *J. Opt. Soc. America A*, vol. 30, no. 6, pp. 1261-1272, 2013.

[21] L. Poli, G. Oliveri, F. Viani, and A. Massa, "MT-BCS-based microwave imaging approach through minimum-norm current expansion," *IEEE Trans. Antennas Propag.*, vol. 61, no. 9, pp. 4722-4732, Sep. 2013.

[22] F. Viani, L. Poli, G. Oliveri, F. Robol, and A. Massa, "Sparse scatterers imaging through approximated multitask compressive sensing strategies," *Microwave Opt. Technol. Lett.*, vol. 55, no. 7, pp. 1553-1558, Jul. 2013.

[23] L. Poli, G. Oliveri, P. Rocca, and A. Massa, "Bayesian compressive sensing approaches for the reconstruction of two-dimensional sparse scatterers under TE illumination," *IEEE Trans. Geosci. Remote Sensing*, vol. 51, no. 5, pp. 2920-2936, May 2013.

[24] L. Poli, G. Oliveri, and A. Massa, "Microwave imaging within the first-order Born approximation by means of the contrast-field Bayesian compressive sensing," *IEEE Trans. Antennas Propag.*, vol. 60, no. 6, pp. 2865-2879, Jun. 2012.

[25] G. Oliveri, A. Randazzo, M. Pastorino, and A. Massa,"Electromagnetic imaging within the contrast-source formulation by means of the multiscaling inexact Newton method," *J. Opt. Soc. America A*, vol. 29, no. 6, pp. 945-958, 2012.

[26] G. Oliveri, L. Poli, P. Rocca, and A. Massa, "Bayesian compressive optical imaging within the Rytov approximation," *Optics Letters*, vol. 37, no. 10, pp. 1760-1762, 2012.

[27] G. Oliveri, P. Rocca, and A. Massa, "A Bayesian compressive sampling-based inversion for imaging sparse scatterers," *IEEE Trans. Geosci. Remote Sensing*, vol. 49, no. 10, pp. 3993-4006, Oct. 2011.

[28] G. Oliveri, Y. Zhong, X. Chen, and A. Massa, "Multi-resolution subspace-based optimization method for inverse scattering," *J. Opt. Soc. America A*, vol. 28, no. 10, pp. 2057-2069, Oct. 2011.

[29] A. Randazzo, G. Oliveri, A. Massa, and M. Pastorino, "Electromagnetic inversion with the multiscaling inexact-Newton method - Experimental validation," *Microwave Opt. Technol. Lett.*, vol. 53, no. 12, pp. 2834-2838, Dec. 2011.

[30] M. Benedetti, D. Lesselier, M. Lambert, and A. Massa, "Multiple shapes reconstruction by means of multi-region level sets," *IEEE Trans. Geosci. Remote Sensing*, vol. 48, no. 5, pp. 2330-2342, May 2010.

[31] M. Benedetti, D. Lesselier, M. Lambert, and A. Massa, "A multi-resolution technique based on shape optimization for the reconstruction of homogeneous dielectric objects," *Inverse Problems*, vol. 25, no. 1, pp. 1-26, Jan. 2009.